Wu *et al. Satellite Navigation* (2024) 5:8
https://doi.org/10.1186/s43020-024-00128-7

Satellite Navigation
https://satellite-navigation.springeropen.com/

ORIGINAL ARTICLE Open Access

Orbit and clock products for quad-system satellites with undifferenced ambiguity fixing approach

Jiaqi Wu[1], Xingxing Li[1], Yongqiang Yuan[1,2*], Keke Zhang[1], Xin Li[1], Jiaqing Lou[1] and Yun Xiong[3,4]

Abstract

Integer Ambiguity Resolution (IAR) can significantly improve the accuracy of GNSS Precise Orbit Determination (POD). Traditionally, the IAR in POD is achieved at the Double Differenced (DD) level. In this contribution, we develop an Un-Differenced (UD) IAR method for Global Positioning System (GPS)+BeiDou Navigation Satellite System (BDS)+Galileo navigation satellite system (Galileo)+Global'naya Navigatsionnaya Sputnikovaya Sistema (GLONASS) quad-system POD by calibrating UD ambiguities in the raw carrier phase and generating the so-called carrier range. Based on this method, we generate the UD ambiguity-fixed orbit and clock products for the Wuhan Innovation Application Center (IAC) of the International GNSS Monitoring and Assessment System (iGMAS). One-year observations in 2020 from 150 stations are employed to investigate performance of orbit and clock products. Notably, the UD Ambiguity Resolution (AR) yields more resolved integer ambiguities than the traditional DD AR, scaling up to 9%, attributable to its avoidance of station baseline formation. Benefiting from the removal of ambiguity parameters, the computational efficiency of parameter estimation undergoes a substantial 70% improvement. Compared with the float solution, the orbit consistencies of UD AR solution achieve the accuracy of 1.9, 5.2, 2.8, 2.1, and 2.7 cm for GPS, BeiDou-2 Navigation Satellite System (BDS-2), BeiDou-3 Navigation Satellite System (BDS-3), Galileo, and GLONASS satellites respectively, reflecting enhancements of 40%, 24%, 54%, 34%, and 42%. Moreover, the standard deviations of Satellite Laser Ranging (SLR) residuals are spanning 2.5–3.5 cm, underscoring a comparable accuracy to the DD AR solution, with discrepancies below 5%. A notable advantage of UD AR lies in its capability to produce the Integer Recovered Clock (IRC), facilitating Precise Point Positioning (PPP) AR without requiring additional Uncalibrated Phase Delay (UPD) products. To assess the performance of quad-system kinematic PPP based on IRC, a network comprising 120 stations is utilized. In comparison to the float solution, the IRC-based PPP AR accelerates convergence time by 31% and enhance positioning accuracy in the east component by 54%.

Keywords Multi-GNSS, Precise orbit determination, Integer recover clock, Undifferenced ambiguity resolution, iGMAS innovation application center

*Correspondence:
Yongqiang Yuan
yqyuan@sgg.whu.edu.cn
Full list of author information is available at the end of the article

Introduction

Considering the swift evolution of Global Navigation Satellite System (GNSS), China established the International GNSS Monitoring and Assessment System (iGMAS) to monitor and evaluate the performance and operational status of GNSS constellations (Chen et al., 2015). As one of the Innovation Application Centers (IAC) of iGMAS, Wuhan University has actively contributed to the quad-system precise products for Global Positioning System (GPS), BeiDou Navigation Satellite System (BDS), Galileo navigation satellite system (Galileo), Global'naya Navigatsionnaya Sputnikovaya Sistema (GLONASS) satellites since June 2020, encompassing precise orbits, clocks, and biases (Li et al., 2022c).

An essential aspect in precise GNSS data processing is the resolution of the integer ambiguity unknowns in phase observations, which significantly impacts the accuracy and reliability of GNSS data processing (Dong & Bock, 1989; Teunissen, 1995; Li et al., 2022a). Traditionally, Integer Ambiguity Resolution (IAR) is achieved at the Double Differenced (DD) level, whereby the phase ambiguities are differenced between receiver pairs and satellite pairs to eliminate hardware delays, yielding readily fixable DD ambiguities (Blewitt, 1989; Ge et al., 2005). In recent years, novel methods have emerged to achieve IAR at the Un-Differenced (UD) level for a single receiver, obviating the need to form baselines. These methods include the Uncalibrated Phase Delay (UPD) model, the decoupled clock model, and the Integer-Recovered Clock (IRC) model (Collins, 2008; Ge et al., 2008; Laurichesse et al., 2009; Li et al., 2013, 2018). These methods calibrate the hardware delays through a least square adjustment utilizing the data from a GNSS reference network and subsequently apply the corrections at each station. This means the UD AR is a technique processing the single-receiver data relative to a network solution. Teunissen and Khodabandeh (2015) demonstrated that the single receiver's integer ambiguity is actually the double-differenced ambiguity. Therefore, single-receiver AR is an undifferenced analysis strategy alternative to the traditional DD AR strategy (Schaer et al., 2021).

One prominent advantage of UD AR lies in its efficient station-by-station processing without baseline formation (Blewitt et al., 2010). Through calibrating resolved integer ambiguities, raw carrier phase can be converted to ambiguity-free observations, known as carrier range, significantly enhancing computational efficiency for undifferenced GNSS data processing. For instance, GPS Precise Orbit Determination (POD) with carrier ranges demonstrated a fivefold improvement over traditional methods when applied to 460 GNSS stations (Chen et al., 2014), and the 5-s interval real-time GPS+Galileo POD can be achieved with UD AR (Dai et al., 2022). Moreover, Chen et al. (2014) demonstrated that the UD AR can improve the GPS orbit overlap accuracy compared with the traditional DD AR by 10%, owing to the enhancement for the continuity of phase observation. Deng et al. (2022) illustrated that the 6-h orbit prediction precision of UD AR solution was improved by 9%-25% compared with DD AR solution. Furthermore, researches suggested that UD AR can offer higher fixing rates and enhance the robustness in quality control compared to conventional approaches (Geng & Mao, 2021; Ruan & Wei, 2019).

Another advantage of UD AR lies in its ability to generate IRC products, facilitating single-receiver AR at the user end (Loyer et al., 2012). This approach has demonstrated a substantial improvement in the convergence speed and positioning accuracy of Precise Point Positioning (PPP) and POD for Low Earth Orbit (LEO) satellites (Laurichesse, 2011; Li et al., 2019a; Montenbruck et al., 2021; Zhang et al., 2021). Thus, to generate the high-precision UD-fixed orbit and IRC products, more and more analysis centers within the International GNSS Service (IGS), such as the Centre National d' Etudes Spatiales (CNES) and Collecte Localisation Satellites (CLS), the Center for Orbit Determination in Europe (CODE), Wuhan University, and GeoForschungsZentrum (GFZ), have adopted the UD AR method (Deng et al., 2022; Geng et al., 2019; Katsigianni et al., 2019; Schaer et al., 2021).

However, previous studies primarily focused on UD AR for GPS or GPS+Galileo POD, while few studies investigated the UD AR POD method for the emerging BeiDou-3 Navigation Satellite System (BDS-3) and GLONASS satellites that transmit Frequency Division Multiple Access (FDMA) signals. As a result, the GPS+BDS+Galileo+GLONASS quad-system UD ambiguity-fixed orbit and IRC products are currently not available. Thus, it is imperative to evaluate the accuracy of quad-system UD ambiguity-fixed orbit and IRC products, as well as the IRC-based PPP. Moreover, previous studies have underscored the enhancement of UD AR over the float solution. However, the performance differences and underlying reasons between UD AR and DD AR methods need analyzing, particularly in multi-GNSS scenarios.

In this contribution, a UD AR method for quad-system POD and PCE is developed by calibrating UD ambiguities in the raw carrier phase and generating the so-called carrier range. Based on this method, the iGMAS Wuhan IAC produces quad-system UD ambiguity-fixed orbit and clock products, an alternative to the traditional DD ambiguity-fixed products. This article provides the theoretical background, strategies, and the validation results of the new UD ambiguity-fixed products. Moreover, it offers a comprehensive comparison and analysis between the UD AR and the traditional DD AR methods concerning the generation of quad-system orbit and clock products.

Following this introduction, "Method" section demonstrates the quad-system GNSS UD AR methods, while "Data and process strategy" section elucidates the GNSS data and the processing strategies adopted in this study. Then, "Results" section presents the experimental validation and resultant analyses. Finally, the conclusions are summarized in "Conclusions" section.

Method

Multi-GNSS observation model

The observation models for GNSS pseudorange P and carrier phase L can be expressed as follows (unit: meter),

$$\begin{aligned} P^s_{r,n} &= \rho^s_r + t_r - t^s + \gamma_n \cdot I^s_{r,1} + b_{r,n} - b^s_n + e^s_{r,n} \\ L^s_{r,n} &= \rho^s_r + t_r - t^s - \gamma_n \cdot I^s_{r,1} + B_{r,n} - B^s_n + \lambda_n \cdot N^s_{r,n} + \varepsilon^s_{r,n} \end{aligned} \tag{1}$$

where s and r refer to satellite and receiver, respectively; n is the frequency; ρ^s_r denote the geometric distance between the phase centers of GNSS transmitter and receiver antenna, also including tropospheric delay, relativistic effects, etc.; t_r is the receiver clock offsets; t^s denotes the satellite clock offsets; $I^s_{r,1}$ refers to the slant ionospheric delay; γ_n is expressed as $\frac{f_1^2}{f_n^2}$; b and B denote the pseudorange and carrier phase hardware delays, respectively; λ_n is the wavelength; $N^s_{r,n}$ is the integer phase ambiguity in cycles; $e^s_{r,n}$ and $\varepsilon^s_{r,n}$ refer to the sum of multipath errors and measurement noise.

To eliminate the first-order ionospheric delay, the Ionosphere-Free Combination (IFC) is widely used in GNSS data processing. The GPS+BDS+Galileo+GLONASS combined IFC observation model is expressed as,

$$\begin{cases} P^{\mathrm{G}}_{r,\mathrm{IF}} = \rho^{\mathrm{G}}_r + \hat{t}_{r,\mathrm{IF}} - \hat{t}^{\mathrm{G}}_{\mathrm{IF}} + e^{\mathrm{G}}_{r,\mathrm{IF}} \\ P^{\mathrm{C}}_{r,\mathrm{IF}} = \rho^{\mathrm{C}}_r + \hat{t}_{r,\mathrm{IF}} - \hat{t}^{\mathrm{C}}_{\mathrm{IF}} + \omega_{\mathrm{C-G}} + e^{\mathrm{C}}_{r,\mathrm{IF}} \\ P^{\mathrm{E}}_{r,\mathrm{IF}} = \rho^{\mathrm{E}}_r + \hat{t}_{r,\mathrm{IF}} - \hat{t}^{\mathrm{E}}_{\mathrm{IF}} + \omega_{\mathrm{E-G}} + e^{\mathrm{E}}_{r,\mathrm{IF}} \\ P^{\mathrm{R}_k}_{r,\mathrm{IF}} = \rho^{\mathrm{R}_k}_r + \hat{t}_{r,\mathrm{IF}} - \hat{t}^{\mathrm{R}_k}_{\mathrm{IF}} + \omega_{\mathrm{R}_k\mathrm{-G}} + e^{\mathrm{R}_k}_{r,\mathrm{IF}} \\ L^{\mathrm{G}}_{r,\mathrm{IF}} = \rho^{\mathrm{G}}_r + \hat{t}_{r,\mathrm{IF}} - \hat{t}^{\mathrm{G}}_{\mathrm{IF}} + \hat{N}^{\mathrm{G}}_{r,\mathrm{IF}} + \varepsilon^{\mathrm{G}}_{r,\mathrm{IF}} \\ L^{\mathrm{C}}_{r,\mathrm{IF}} = \rho^{\mathrm{C}}_r + \hat{t}_{r,\mathrm{IF}} - \hat{t}^{\mathrm{C}}_{\mathrm{IF}} + \hat{N}^{\mathrm{C}}_{r,\mathrm{IF}} + \omega_{\mathrm{C-G}} + \varepsilon^{\mathrm{C}}_{r,\mathrm{IF}} \\ L^{\mathrm{E}}_{r,\mathrm{IF}} = \rho^{\mathrm{E}}_r + \hat{t}_{r,\mathrm{IF}} - \hat{t}^{\mathrm{E}}_{\mathrm{IF}} + \hat{N}^{\mathrm{E}}_{r,\mathrm{IF}} + \omega_{\mathrm{E-G}} + \varepsilon^{\mathrm{E}}_{r,\mathrm{IF}} \\ L^{\mathrm{R}_k}_{r,\mathrm{IF}} = \rho^{\mathrm{R}_k}_r + \hat{t}_{r,\mathrm{IF}} - \hat{t}^{\mathrm{R}_k}_{\mathrm{IF}} + \hat{N}^{\mathrm{R}_k}_{r,\mathrm{IF}} + \omega_{\mathrm{R}_k\mathrm{-G}} + \varepsilon^{\mathrm{R}_k}_{r,\mathrm{IF}} \end{cases} \tag{2}$$

with

$$\begin{cases} \hat{t}_{r,\mathrm{IF}} = t_r + b^{\mathrm{G}}_{r,\mathrm{IF}} \\ \hat{t}^s_{\mathrm{IF}} = t^s + b^s_{\mathrm{IF}} \\ \omega_{X\mathrm{-G}} = b^X_{r,\mathrm{IF}} - b^{\mathrm{G}}_{r,\mathrm{IF}} \\ \hat{N}^s_{r,\mathrm{IF}} = N^s_{r,\mathrm{IF}} + (B_{r,\mathrm{IF}} - b_{r,\mathrm{IF}}) - (B^s_{\mathrm{IF}} - b^s_{\mathrm{IF}}) \end{cases} \tag{3}$$

where the superscripts G, C, E, and R_k denote the GPS, BDS, Galileo, and GLONASS satellites, respectively; subscripts k in R_k is the GLONASS channel number; $N^s_{r,\mathrm{IF}}$ is the IFC ambiguity in meter; $\omega_{X-\mathrm{G}}$ denote the pseudorange Inter-System Biases (ISB) among BDS, Galileo, GLONASS and GPS. Considering the hardware delays for different GLONASS satellites vary with their channel number k, the GLONASS Inter-Frequency Bias (IFB) $\omega_{\mathrm{R}_k-\mathrm{G}}$ is estimated for each GLONASS channel.

There are two singularities in this linear system caused by the satellite clock and ISB parameters. In this study, all the clock offsets are defined relative to a selected station with its GPS receiver clock offsets arbitrarily fixed to zero. Reference stations are also selected for other systems to fasten their ISBs to zero (Li et al., 2015).

Undifferenced ambiguity resolution

As illustrated in Eq. (3), the estimated ambiguity $\hat{N}$ loses its integer property due to the phase and code delays. Consequently, we must eliminate the satellite and receiver UPDs absorbed in the ambiguity parameter to achieve the UD AR. Since the estimated IFC ambiguity is not naturally an integer, the Wide-Lane (WL) and Narrow-Lane (NL) ambiguities (N_1 in this study) are adopted in IAR,

$$\begin{cases} \dfrac{1}{\lambda_{\mathrm{NL}}} \cdot N_{\mathrm{IF}} = \dfrac{f_2}{f_1 - f_2} \cdot N_{\mathrm{WL}} + N_1 \\ \lambda_{\mathrm{NL}} = \dfrac{c}{f_1 + f_2} \end{cases} \tag{4}$$

where λ_{NL} is the wavelength of NL ambiguity; N_{WL} denote the WL ambiguity, which can be obtained from the Hatch-Melbourne-Wübbena (HMW) combination (Hatch, 1983; Welbourne, 1985; Wubbena, 1985). Then, the NL ambiguity can be computed with WL and IFC ambiguities.

The UD WL and NL ambiguity parameters can be expressed as a linear combination of the integer value and UPDs,

$$\hat{N}^s_* = N^s_* + \mu_{*,r} - \mu^s_* \tag{5}$$

where subscript $*$ denotes WL or NL; $\hat{N}^s_*$ and N^s_* refer to the ambiguities of float and integer values, respectively; $\mu_{*,r}$ and μ^s_* are the receiver and satellite UPDs.

Assuming there are n stations tracking m satellites, we can estimate the satellite and receiver UPDs by a least square adjustment as follows (Ge et al., 2008; Li et al., 2013),

$$\begin{pmatrix} \delta N_{*,1} \\ \delta N_{*,2} \\ \vdots \\ \delta N_{*,n+m} \end{pmatrix} = (\boldsymbol{I}_n \otimes \boldsymbol{R}_m, -\boldsymbol{R}_n \otimes \boldsymbol{I}_m) \cdot \begin{pmatrix} \mu_{*,r_1} \\ \vdots \\ \mu_{*,r_n} \\ \mu_*^{s_1} \\ \vdots \\ \mu_*^{s_m} \end{pmatrix} \quad (6)$$

where $\delta N_{*,i}$ denotes the fractional part of the float ambiguity, which is computed by $\delta N_{*,i} = \hat{N}_{*,i} - N_{*,i}$; $\boldsymbol{I}_n$ is the identity matrix of dimension n; $\boldsymbol{R}_n$ refers to the vector $(1, 1, \cdots, 1)^{\mathrm{T}}$ with dimension n; $\otimes$ denotes the Kronecker product. To solve the rank deficiency in Eq. (6), a satellite or receiver UPD is selected as the reference and fixed to a prior value. Notably, the receiver UPD for a specific receiver $\mu_{*,r}$ varies with different GNSS systems. As a consequent, the UPD should be separately estimated for each system (Li et al., 2018, 2022b). Specially, the IFB of a particular GLONASS satellite varies with the receivers' manufacturers, antennas, domes, and even firmware, so the GLONASS UPD estimation is usually utilized with homogeneous receivers (Liu et al., 2017).

Based on the above algorithm, the satellite UPD can be precisely estimated using around 100 globally distributed stations. For a single-receiver user, the integer property can be recovered for Single-Differenced (SD) ambiguity by correcting the satellite UPD and making the difference between two UD ambiguities from different satellites,

$$\Delta N_*^{s_1,s_2} = \hat{N}_*^{s_1} - \hat{N}_*^{s_2} - \mu^{s_1} + \mu^{s_2} \quad (7)$$

where subscripts s_1 and s_2 are two different satellites. Subsequently, the integer values of SD ambiguities can be resolved through a rounding or search strategy (Dong & Bock, 1989; Teunissen, 1995).

To further obtain the integer UD ambiguities, we select a UD ambiguity with the highest precision as the datum and directly fix it to the nearest integer value after correcting satellite UPD. Then, an independent subset of SD ambiguities is selected by their fixing probability (Ge et al., 2005). Subsequently, all the UD ambiguities can be resolved as,

$$\begin{pmatrix} N_*^{\mathrm{ref}} \\ \Delta N_*^{s_1,s_2} \\ \Delta N_*^{s_1,s_3} \\ \vdots \\ \Delta N_*^{s_j,s_k} \end{pmatrix} = \begin{pmatrix} 1 & 0 & 0 & \cdots & 0 \\ 0 & 1 & -1 & \cdots & 0 \\ \vdots & \vdots & \vdots & & \vdots \\ 0 & 0 & 0 & \cdots & -1 \end{pmatrix} \cdot \begin{pmatrix} N_*^{\mathrm{ref}} \\ N_*^{s_1} \\ N_*^{s_2} \\ \vdots \\ N_*^{s_k} \end{pmatrix} \quad (8)$$

where N_*^{ref} is the datum UD ambiguity; the design matrix is a full-rank square matrix with $1, -1$, and 0.

By correcting the integer WL and NL ambiguities, a raw phase observation can be converted to a carrier range as follows (Blewitt et al., 2010; Chen et al., 2014),

$$\tilde{L}_{r,\mathrm{IF}}^s = L_{r,\mathrm{IF}}^s - \lambda_{\mathrm{NL}} \cdot \left(\frac{f_2}{f_1 - f_2} \cdot N_{r,\mathrm{WL}}^s + N_{r,1}^s \right) \quad (9)$$

The carrier range is an unambiguous phase observation, like high precision pseudorange measurement. Therefore, the pseudorange observation becomes unnecessary when applying carrier range. The ameliorated multi-GNSS observation model based on carrier range can be expressed as:

$$\begin{cases} \tilde{L}_{r,\mathrm{IF}}^{\mathrm{G}} = \rho_r^{\mathrm{G}} + \tilde{t}_{r,\mathrm{IF}} - \tilde{t}_{\mathrm{IF}}^{\mathrm{G}} + \varepsilon_{r,\mathrm{IF}}^{\mathrm{G}} \\ \tilde{L}_{r,\mathrm{IF}}^{\mathrm{E}} = \rho_r^{\mathrm{E}} + \tilde{t}_{r,\mathrm{IF}} - \tilde{t}_{\mathrm{IF}}^{\mathrm{E}} + \tilde{\omega}_{\mathrm{E-G}} + \varepsilon_{r,\mathrm{IF}}^{\mathrm{E}} \\ \tilde{L}_{r,\mathrm{IF}}^{\mathrm{C}} = \rho_r^{\mathrm{C}} + \tilde{t}_{r,\mathrm{IF}} - \tilde{t}_{\mathrm{IF}}^{\mathrm{C}} + \tilde{\omega}_{\mathrm{C-G}} + \varepsilon_{r,\mathrm{IF}}^{\mathrm{C}} \\ \tilde{L}_{r,\mathrm{IF}}^{\mathrm{R}_k} = \rho_r^{\mathrm{R}_k} + \tilde{t}_{r,\mathrm{IF}} - \tilde{t}_{\mathrm{IF}}^{\mathrm{R}_k} + \tilde{\omega}_{\mathrm{R}_k-\mathrm{G}} + \varepsilon_{r,\mathrm{IF}}^{\mathrm{R}_k} \end{cases} \quad (10)$$

with

$$\begin{cases} \tilde{t}_{r,\mathrm{IF}} = t_r + B_{r,\mathrm{IF}}^{\mathrm{G}} \\ \tilde{t}_{\mathrm{IF}}^s = t^s + B_{\mathrm{IF}}^s \\ \tilde{\omega}_{X-\mathrm{G}} = B_{r,\mathrm{IF}}^X - B_{r,\mathrm{IF}}^{\mathrm{G}} \end{cases} \quad (11)$$

where $\tilde{\omega}_{X-\mathrm{G}}$ and $\tilde{t}_{r,\mathrm{IF}}$ are the carrier phase ISB and clock offsets. Due to the removal of ambiguity parameters, the receiver and satellite phase delays are obliged to be absorbed by ISB and clock estimates. Different from the legacy code clock $\hat{t}_{\mathrm{IF}}^s$ in Eq. (2), the obtained phase clock $\tilde{t}_{\mathrm{IF}}^s$, also known as the integer clock, can support users to achieve single-receiver ambiguity resolution without extra UPD products (Geng et al., 2019; Laurichesse et al., 2009; Loyer et al., 2012; Schaer et al., 2021).

Data and processing strategy

Multi-GNSS constellations and tracking networks

Currently, more than 120 GNSS satellites are operational, transmitting navigation signals to global users. With the modernization of GPS and GLONASS, six GPS Block III and four GLONASS-K1 satellites were launched. The current GPS and GLONASS constellations comprise 31 and 24 operational satellites, respectively. Since July 31, 2020, the Chinese BDS-3 has provided fully operational global services, with the entire constellation consisting of 30 satellites, including 3 GEostationary Orbit (GEO), 3 Inclined GeoSynchronous Orbit (IGSO), and 24 Medium Earth Orbit (MEO) satellites (Yang et al., 2021). The current Galileo constellation comprises 22 fully operational satellites, 2 testing satellites on improper orbits, and 3

Table 1 Deployment status of the multi-GNSS constellations as of July 2023

System	Blocks	Signals	Satellites
GPS	IIR	L1C/A, L1/L2 P(Y)	7
	IIR-M	L1C/A, L1/L2 P(Y), L2C, L1/L2 M	7
	IIF	L1C/A, L1/L2 P(Y), L2C, L1/L2 M, L5	12
	III	L1C, L1C/A, L1/L2 P(Y), L2C, L1/L2 M, L5	5 + 1[a]
BDS-2	GEO	B1I, B2I, B3I	5
	IGSO	B1I, B2I, B3I	7
	MEO	B1I, B2I, B3I	3
BDS-3	GEO	B1I, B3I, B2b	2 + 1[a]
	IGSO	B1I, B3I, B1C, B2a/b	3
	MEO	B1I, B3I, B1C, B2a/b	24
Galileo	IOV	E1, E6, E5a/b/ab	3 + 1[a]
	FOC	E1, E6, E5a/b/ab	19 + 4[a]
GLONASS	M	L1/L2 C/A + P	15
	M +	L1/L2 C/A + P, L3	6
	K	L1/L2 C/A + P, L3	3 + 1[a]

[a] Non-operational satellite

unserviceable satellites (Hadas et al., 2019). Table 1 provides a comprehensive overview of the current deployment status of multi-GNSS constellations, delineating satellite block types, transmitted signal types, and the number of available satellites as of July 2023.

We employed the observations of one year at 150 IGS Multi-GNSS Experiment (MGEX) stations in 2020 to conduct GPS + BDS + Galileo POD. All these stations enable to track both GPS and Galileo dual-frequency signals, while about 120 of them can also track the collaborative B1I/B3I signals of BDS-2 and BDS-3. Since the code and phase IFB of a specific GLONASS satellite vary with receiver types (Yamada et al., 2010), we adopted a network comprising homogeneous receivers for both DD and UD AR (Liu et al., 2017). Hence, we selected all available MGEX stations equipped with SEPT POLARX5 receivers (103 stations) to execute GPS + GLONASS POD utilizing the data in the same period.

Figure 1 illustrates the distribution of selected stations utilized for the multi-GNSS POD. The POD process used all available GPS, Galileo, GLONASS, BDS-2 IGSO/MEO satellites, and a significant portion of the BDS-3 MEO satellites. However, the BDS GEO satellites were excluded due to their frequent orbit maneuvers and unfavorable observational geometry. In the selected period, the observations for BDS-3 satellites with PRN larger than C37 are insufficient, so C38-C46 were also not used. Besides, R06 and R10 were not used due to the lack of dual-frequency observations.

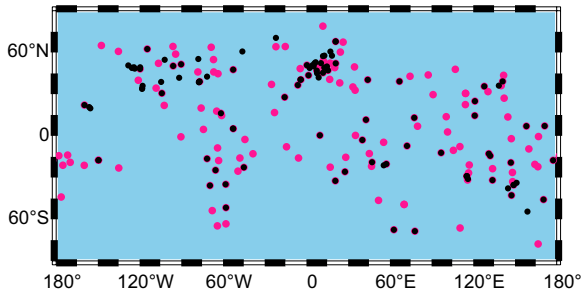

Fig. 1 Distribution of the selected MGEX stations utilized for the multi-GNSS POD} (pink dots: stations for GPS + BDS + Galileo POD; black dots: stations equipped with SEPT POLARX5 receivers for GPS + GLONASS POD

POD strategy

In this study, we utilized the GREAT (GNSS + REsearch, Application, and Teaching) software, developed by Wuhan University, for processing the quad-system GNSS data (Li et al., 2021, 2023). Table 2 summarizes the detailed POD strategy. The UD IFC pseudorange and carrier phase formed by L1/L2 for GPS and GLONASS, E1/E5a for Galileo, and B1I/B3I for BDS were adopted in the POD. The a priori noises are 0.6 m for pseudorange and 0.01 cycles for carrier phase. Empirically, the a priori pseudorange noises of GLONASS are set to 3.0 m due to relatively lower pseudorange precision. The satellite-induced code bias of BDS-2 satellites is calibrated with the existing models (Wanninger & Beer, 2015). The POD arc is 24 h with a sampling interval of 300 s. As to the Solar Radiation Pressure (SRP) models, the well-proved ECOM2 (9 parameters), ECOM (5 parameters), and the a priori box-wing model were employed for GPS/GLONASS, BDS, and Galileo POD, respectively (Arnold et al., 2015; Li et al., 2019b; Montenbruck et al., 2015; Springer et al., 1999).

Considering the code hardware delays originated in receiver vary with different systems and channels, the ISB of Galileo and BDS and IFB of GLONASS relative to GPS were estimated as constants for each 24-h arc. It was also reported that the ISB exists between BDS-2 and the newly complete BDS-3 (Zhao et al., 2020). Hence, BDS-3 and BDS-2 are treated as two systems in parameter estimation and ambiguity resolution, which means that the differential ambiguity will not be formed between BDS-3 and BDS-2 satellites.

To validate the proposed method, the traditional DD ambiguity-fixed orbit and clock products are also processed for comparison. The same DD AR strategy is used as Ge et al. (2005). Figure 2 shows the processing procedure for POD. The daily POD is processed in the following steps to ensure that all the experimental solutions use

Table 2 Processing strategy for multi-GNSS POD

Items	Strategies
Observation model	
Observations	Undifferenced IFC pseudo-range and carrier phaseGPS: L1/L2; Galileo: E1/E5a; BDS: B1I/B3I; GLONASS: L1/L2
A prior noise	Pseudo-range: 0.6, 0.6, 0.6, and 3.0 m for GPS, Galileo, BDS, and GLONASS, respectively Carrier phase: 0.01 cycles
Weighting	Elevation-dependent weighting with 7° cutoff
POD arc	24 h arc length, 300 s sampling
Satellite antenna	igs14.atx
Receiver antenna	igs14.atx
Phase-windup effect	Corrected
Tropospheric delay	The priori delays are computed with Saastamoinen model (Saastamoinen, 1972) and Global Mapping Function (Böhm et al., 2006); then, the residual delays are estimated as piecewise constant function every 2 h
Station coordinates	Tightly constraint to IGS weekly solutions
Dynamic model	
Earth gravity field	12×12 EGM2008 model (Pavlis et al., 2012)
N-body gravitation	Planetary and lunar ephemeris DE 421 (Folkner et al., 2009)
Ocean tides	FES 2004 (Lyard et al., 2006)
Solid earth and pole tides	IERS conventions 2010 (Luzum & Petit, 2012)
Relativity effect	IERS conventions 2010
Antenna thrust	Correct (Steigenberger et al., 2018)
Solar radiation pressure	GPS/GLONASS: ECOM2; BDS: ECOM; Galileo: ECOM + the a prior box-wing model
Estimated parameters	
Estimator	Sequential least square adjustment
Initial state	Satellite position and velocity at initial epoch
Dynamic parameters	SRP parameters
Satellite clock offset	Epoch-wisely estimated as white noise
Receiver clock offset	Epoch-wisely estimated as white noise; Estimate ISB of Galileo, BDS-3, BDS-2, and IFB of GLONASS channels as constants
Phase ambiguities	Constant over each continuous observation arc
Earth rotation parameters	Estimating Xpole, DXpole, Ypole, DYpole, DUT1, with UT1 fixed

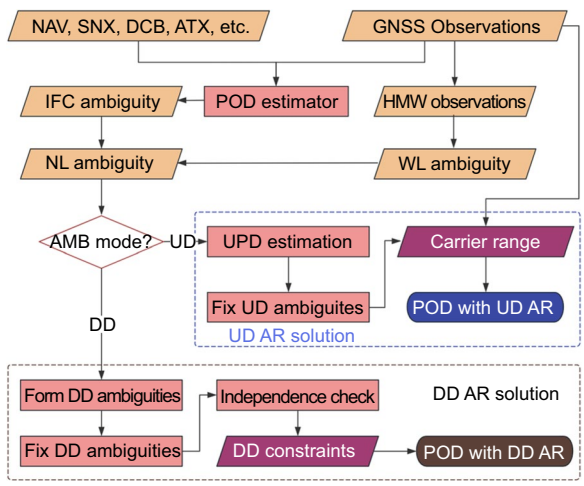

Fig. 2 Flowchart of POD using UD and DD AR solutions

the same input information: (1) the multi-GNSS POD is implemented iteratively till the convergence is achieved to generate the float IFC and WL ambiguities; (2) the DD and UD ambiguities are fixed to integer values with different ambiguity resolution methods; (3) apply the DD ambiguity constraints or carrier ranges to the POD estimators and achieve ambiguity-fixed solutions. The ambiguities which are not fixed in the UD approach will be estimated as real numbers in step (3).

Results

Ambiguity fixing performance

High-quality WL and NL UPD products play a crucial role in the UD ambiguity resolution process. Previous research has demonstrated that the WL UPDs remain stable for several months, whereas the NL UPDs are stable within several hours (Ge et al., 2008; Li et al., 2018).

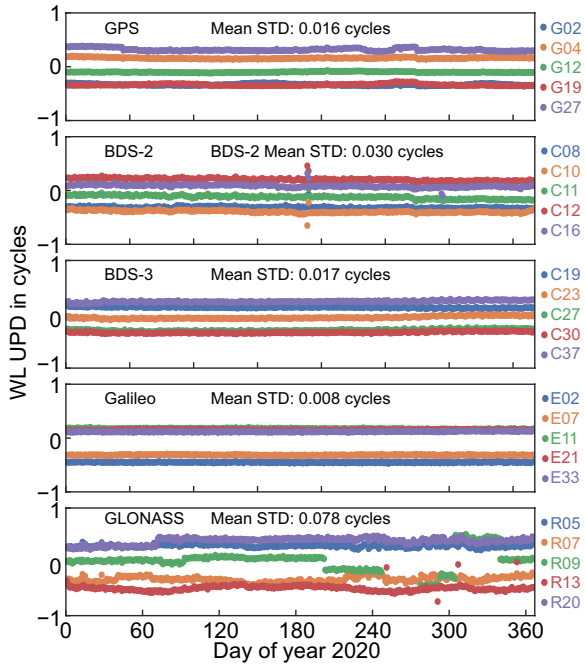

Fig. 3 Time series of multi-GNSS WL UPDs in 2020

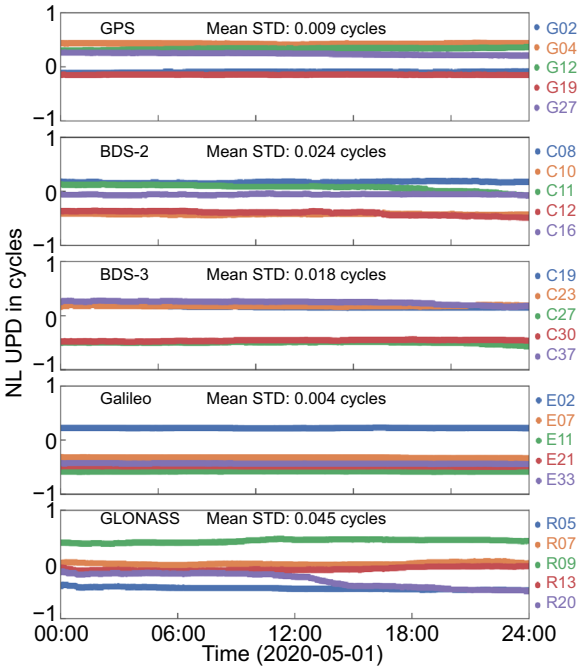

Fig. 4 Time series of multi-GNSS NL UPDs at 2020–05-01

Figure 3 depicts the time series of multi-GNSS WL UPDs in 2020. It is observed that Galileo, GPS, and BDS-3 satellites exhibit excellent stability, with a STandard Deviation (STD) of smaller than 0.02 cycles. The BDS-2 WL UPD series exhibit frequent but slight fluctuations, which could be attributed to the pseudo-range noise and other unmodeled biases. Several large jumps and discontinuities are observed for R09, which may be due to regular maintenance activities (https://www.glonass-iac.ru/news/news_glonass).

Figure 4 presents the time series of multi-GNSS NL UPDs on 2020–05-01. The results show that all the satellites exhibit excellent stability with STD values smaller than 0.08 cycles. Once again, the performance of Galileo, GPS, and BDS-3 is the best, followed by BDS-2 and GLONASS. The poorer quality of WL UPD and lower POD accuracy adversely affects the NL UPD quality of BDS-2 and GLONASS. Furthermore, the inconsistency of GLONASS IFBs among the selected homogeneous receivers may also affect GLONASS NL UPD accuracy.

After correcting the multi-GNSS WL and NL UPDs, the UD AR can be performed station by station. As depicted in Fig. 5, the WL fixing rates are 97–99% and 95–98% for DD AR and UD AR, respectively, while the NL fixing rates are 93–97% and 87–96%. These results demonstrate a good consistency with the previous studies, e.g., Ge et al. (2005), Ge et al. (2008), Li et al. (2018), and Katsigianni et al. (2019).

It is noteworthy that the DD AR displays higher fixing rates but marginally fewer independent ambiguities than UD AR. This is because redundant DD candidates are much more than UD candidates. For instance, for GPS, there are over 330,000 DD candidates from more than 1000 station pairs, whereas the UD candidates are only 60,000. Therefore, the linear independence check selects more easy-to-fix DD ambiguities (Ge et al., 2005). Mathematically, the number of chosen independent DD ambiguities is three less than that of UD ambiguities. However,

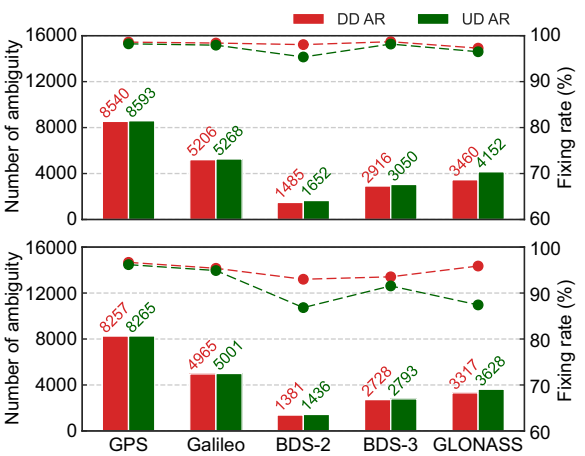

Fig. 5 Fixing rates and the number of successfully fixed ambiguities for DD AR and UD AR

forming DD ambiguity needs two stations simultaneously tracking two satellites for at least a few minutes, which is influenced by the distance and distribution of stations, especially for the areas with sparse stations like open seas, remote areas, etc. In contrast, the UD method is much more flexible because it processes the data of a single receiver. Moreover, the UD method corrected the UPD estimated from a global network, while the DD method eliminated the UPD by the DD operation, which was affected by the distance between the two stations and the quality of their ambiguities (Geng & Mao, 2021). In this context, the difference between NL ambiguity numbers of DD AR and UD AR is less than 1% for GPS and Galileo, owing to their relatively adequate and evenly distributed stations. In contrast, the stations capable of tracking BDS signals are fewer, and the IGSO satellites can only be tracked by regional networks, leading to differences of 2% and 4% for BDS-3 and BDS-2. GLONASS demonstrates the largest difference of 9% since only 103 unevenly distributed stations are selected to satisfy the requirement of homogeneous receivers.

Computational efficiency

With the rapid expansion of GNSS constellations and networks, the computational burden of GNSS network data processing has become a significant challenge. The sequential least squares adjustment method has been widely utilized in precise orbit and clock determination. This method uses Gauss elimination to remove inactive parameters, such as elapsed ambiguities and zenith troposphere delays, and achieve higher efficiency than the batch least square adjustment (Ge et al., 2006). However, the Norm EQuation (NEQ) matrix still has many active ambiguities, and the parameter elimination process is time-consuming. Figure 6 illustrates the number of active parameters per epoch under the assumption that n stations are tracking m satellites, and each station on average observes 1/4 of the available satellites. The results show that ambiguities account for 57% of the NEQ dimension when 100 stations are tracking 120 satellites. This percentage increases to 73% when the number of stations increases to 450.

The carrier range presents a promising approach to significantly enhance computational efficiency in GNSS network data processing by eliminating the ambiguity. The generation of carrier range involves two steps: UPD estimation and UD AR, both of which can be processed quickly. The former step takes less than one minute, while the latter is station-based and can be executed in parallel on multiple processors and computers within five seconds (Chen et al., 2014). Subsequently, the computation time of the sequential least square adjustment can be divided into three parts: parameter elimination, forming NEQ, and solving NEQ. Notably, solving NEQ accounts for less than 0.3% of the total time. As the NEQ dimension is significantly reduced, the carrier range approach is expected to expedite parameter elimination. Additionally, pseudorange is no longer required in the carrier range approach, and only half of the observations need to be processed, resulting in a potential 50% reduction in the computation time of forming NEQ (Blewitt et al., 2010).

For verification purposes, a total of 450 IGS stations were utilized to implement the POD using IFC phase + range observations and carrier ranges of

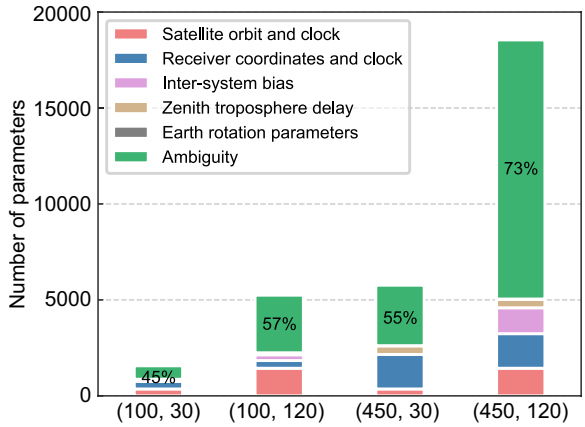

Fig. 6 Number of active parameters per epoch in POD (using ECOM SRP model) for n stations and m satellites, which is marked as (n, m)

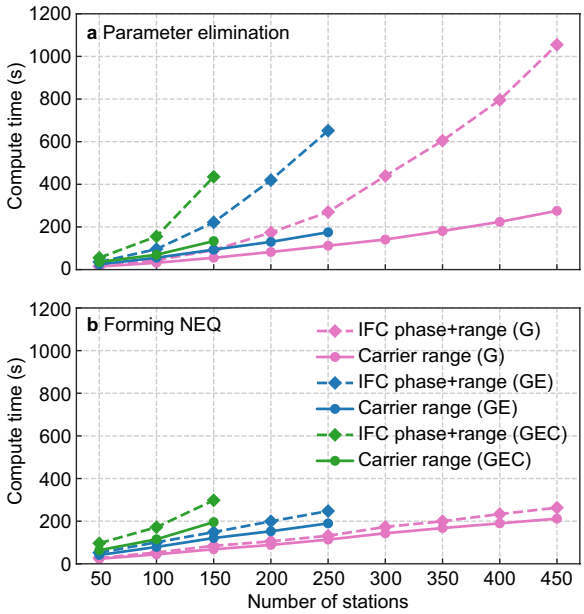

Fig. 7 Computation time of **a** parameter elimination and **b** form norm equation using IFC phase + range observations and carrier range, respectively

DOY135, 2020. It is worth noting that only 277 stations can track Galileo signals, and this number is further reduced to 159 if we consider BDS-3 signals. As illustrated in Fig. 7, the computation time of parameter elimination and forming NEQ increases geometrically and linearly, respectively, and their slopes are amplified with the growing number of satellites. Remarkably, the carrier range approach significantly increases the computational efficiency of parameter elimination compared to the traditional approach. For instance, the both GPS-only strategy with 450 stations and the triple-system strategy with 150 stations resulted in a 70% reduction in the computation time. However, forming NEQ was improved by around 15–30%, which is lower than the expected ideal reduction of 50%. The possible explanation for this discrepancy is that most error models, such as coordinates, clocks, and troposphere delays, are common for both range and phase observations and must be calculated, even though the range observations have been excluded.

Figure 8 illustrates the computation time of the whole DD AR module and UD AR module, including ambiguity fixing and POD parameter estimation. It can be found that the time consumption of DD AR grows dramatically with the increasing of station number, especially for multi-GNSS. In contrast, the UD AR presents a noticeably smaller slope for the time consumption. The GPS-only DD AR module takes 1605 s when there are 450 stations, while the UD AR module takes only 509 s, with the improvements of 68%.

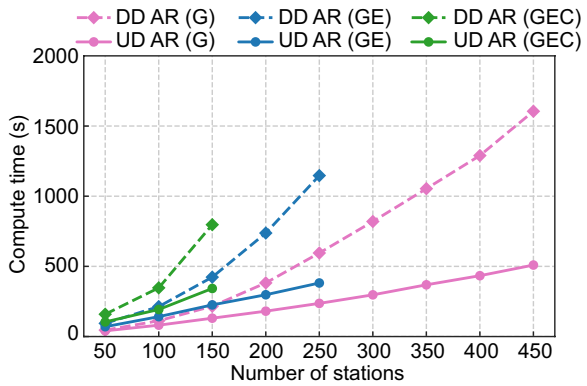

Fig. 8 Computation time of the whole DD AR module and UD AR module

Orbit consistency

We employed the multi-GNSS data of one year in 2020 collected at 150 MGEX stations to evaluate the POD accuracy with UD AR. To assess the consistency of daily solutions, we conducted two-day arc solutions by fitting the orbital parameters through consecutive one-day orbital solutions. The Root Mean Square (RMS) values of the two-day orbit fits were used as indicators of day-to-day orbit consistency. Figure 9 illustrates the 3D RMS values of orbit fits of the float, DD AR, and UD AR solutions. Notable improvements are found when comparing the UD AR solution and float solution. The UD AR solution presents the 3D RMS values of 1.9, 2.1, 2.7, 5.2, and 2.8 cm for GPS, Galileo, GLONASS, BDS-2, and BDS-3 satellites, with the improvements of 40%, 34%, 42%, 24%, and 54%. The performance is slightly better than the DD AR solution, with an improvement of 1–5% for different systems. This result is like the previous studies, e.g., Ruan and Wei (2019); Geng and Mao (2021). Remarkably, all the BDS-3 satellites exhibit a noticeable higher orbit consistency when comparing the UD AR solution with DD AR solution, with an improvement of 3–7%.

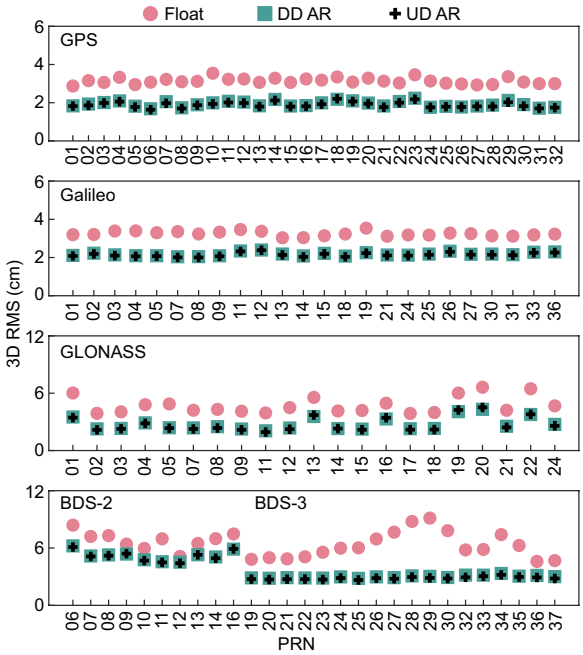

Fig. 9 Average 3D RMS values of orbit fits of float, DD AR, and UD AR solutions

Besides, it is noteworthy that satellites R01, R13, R16, R19, R20, and R22 exhibit much larger RMS values than other GLONASS satellites, aligning with the results by Prange et al. (2017) and Bury et al. (2022). A possible reason is sharing the pre-2011 launch dates of these satellites, engendering a requisite for re-calibration of their antenna phase center corrections (Dach et al., 2019). Therefore, we mark these satellites as GLONASS-Me is this study. Moreover, the float solutions for satellites C27-C30 and C34-C35 (in slot A) manifest notably larger RMS values relative to the satellites in slots B and C. This can be attributed to the sun elevation angles above the orbital

plane in slot A ranging within ±33°, leading to the longer eclipse seasons. Nevertheless, the application of ambiguity resolution significantly improves their orbit consistency to a same level with other BDS-3 MEO satellites.

Orbit comparison

In addition, we compare the estimated orbits with MGEX final orbit products, e.g., COM from CODE (Prange et al., 2017), GBM from GFZ (Uhlemann et al., 2016), WUM from Wuhan University (WHU) (Guo et al., 2016), and ESM from the European Space Agency (ESA) (Montenbruck et al., 2017).

Figure 10 illustrates the 3D RMS values of the orbit differences with respect to different products. The orbit differences of BDS-3 satellites with respect to COM are absent due to the unavailability of CODE's BDS-3 orbits for the year 2020. A substantial reduction of 50% in orbit difference is exhibited for GPS satellites between the float and UD AR solutions. Similarly, Galileo presents a significant improvement of 32–49% in orbit difference by applying UD AR. Nevertheless, the discrepancy between the results of UD AR solution and DD AR solution is smaller than 5%.

For BDS-3 satellites, the disparities in orbit differences within the float solutions remain consistent across various products, hovering around 11 cm. However, the ambiguity-fixed results have notable variations with a shift in median values from ESM's 5.7 cm to WUM's 8.7 cm. This divergence possibly stems from the different ambiguity resolution strategies adopted by different institutions, leading to the accuracy improvement by ambiguity resolution ranging from 14 to 52%. Similar disparities are also observed for BDS-2 satellites across different products, with the median values of the UD AR solution spanning from COM's 21.1 cm to WUM's 10.9 cm. The possible reason resides in the different SRP models employed by these institutions.

Furthermore, the orbit difference of ambiguity-fixed solution for GLONASS satellites exhibit a minimal reduction or even exacerbation compared with GBM, WUM, and ESM products. Nevertheless, a notable reduction in orbit differences concerning COM is manifest, amounting to a marked 38%. This discrepancy can probably be attributed to the fact that COM's GLONASS orbits are ambiguity-fixed solutions (Prange et al., 2017), while the GLONASS orbits from GBM, WUM, and ESM remain the float solutions.

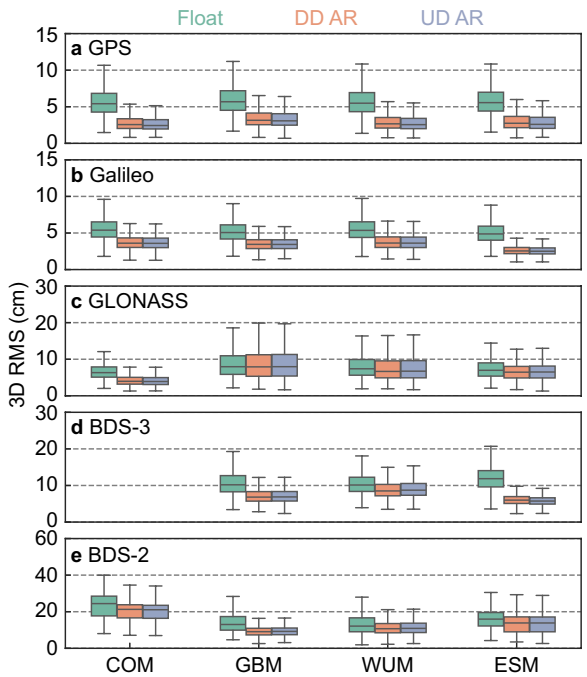

Fig. 10 Statistics on the 3D orbit difference RMS values compared with final orbit products from COM, GBM, WUM, and ESM (from left to right)

SLR validation

Satellite Laser Ranging (SLR) provides an independent distance measurement from SLR stations to satellites with mm-to-cm-level precision. Therefore, the SLR residuals can serve as an external indicator of GNSS orbit accuracy. Currently, all the Galileo and GLONASS satellites and some BDS satellites are tracked by the International Laser Ranging Service (ILRS) (Pearlman et al., 2019). One-year SLR observations in 2020 are employed to compute the SLR residuals. As depicted in Fig. 11, all the 34 available ILRS stations are used for the SLR validation. The outlier threshold is set to ± 0.2 m, and the elevation cutoff is 10°.

Figure 12 presents the time series of SLR residuals for C20 and C29, respectively manufactured by the China Academy of Space Technology (CAST) and Shanghai Engineering Center for Microsatellites (SECM). The SLR residuals maintain temporal stability yet reveal dispersed deviations during eclipse seasons. It is noticeable that

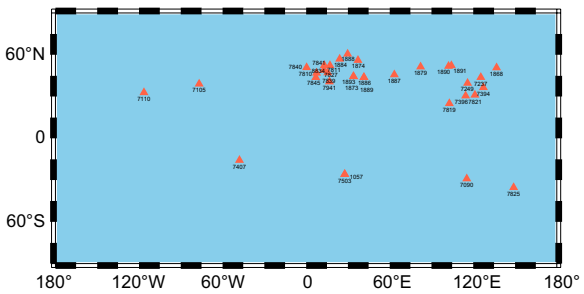

Fig. 11 Distribution of IRLS stations used for SLR validation

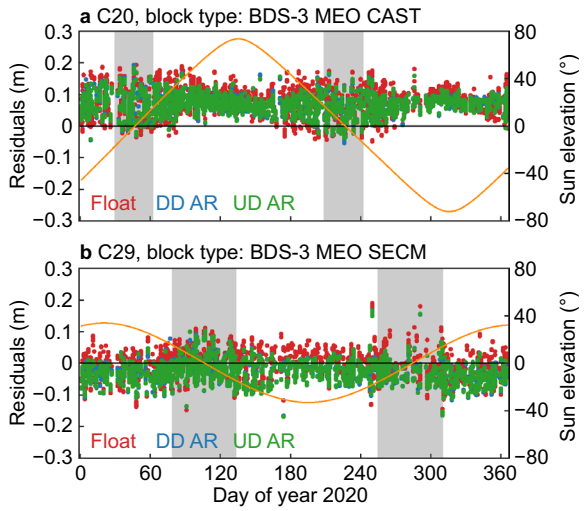

Fig. 12 Time series of SLR residuals for C20 and C29 utilizing float, DD AR, and UD AR solutions. The shaded area indicates the eclipse season

distinct mean biases emerge, with C20 recording 6.7 cm and C29 registering − 2.7 cm, due to the contrasting area ratios between their X-bus and Z-bus surfaces (Zhao et al., 2022). Furthermore, employing UD AR leads to notably diminished scatters compared to the float solution, evidenced by a reduction of STD values from 4.2 and 4.4 cm to 3.1 and 3.5 cm, representing improvements of 28% and 20%, respectively. The results align with the DD AR solution, demonstrating a discrepancy of less than 1%.

Figure 13 illustrates the statistics of SLR residuals for BDS, Galileo, and GLONASS satellites. Compared with the float solutions, the STD values of UD AR solutions exhibit a substantial improvement of 21% for BDS-3 satellites. This is followed by a 10% enhancement for GLONASS satellites and a 5% improvement for Galileo satellites. Notably, the disparity between the UD AR solutions and the DD AR solutions remains insignificant, amounting to less than 3%.

For BDS-2 MEO and BDS-3 MEO satellites the residuals show comparable accuracy of about 3.5 cm when utilizing the UD AR solution. Conversely, for BDS-2 IGSO satellites they exhibit larger scatters, with a STD of 5.9 cm. For Galileo satellites, the UD AR solutions yield a mean STD value of 2.5 cm, while for GLONASS satellites3.3 cm. However, for the GLONASS-Me satellites the residuals deviate significantly with STD value of approximately 7.4 cm, and the application of ambiguity resolution fails to improve orbital accuracy. This is possibly attributable to imprecise antenna phase center corrections (Dach et al., 2019).

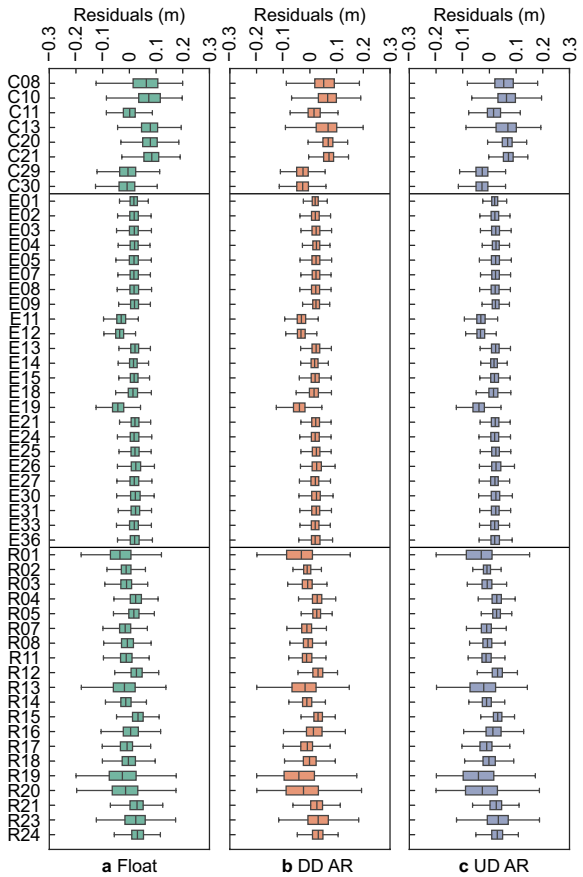

Fig. 13 Statistics on the SLR residuals for BDS, Galileo, and GLONASS satellites. Subgraphs from top the bottom denote **a** float, **b** DD AR, and **c** UD AR solutions

Clock comparison

To validate the generated precise clock products, we compare them with the final products from COM, GBM, WUM, ESM. The clock time series are aligned to a reference satellite to eliminate the systematic errors in clock comparisons (Ge et al., 2012).

Figure 14 illustrates the mean STD values of clock differences for different systems. The UD AR solution demonstrates a remarkable consistency with the precise products for GPS and Galileo satellites, the mean STD values ranging from 0.07 to 0.10 ns, with an improvement of approximately 25% compared with the float solution. Noteworthy a progress is also observed for BDS-3 satellites with the mean STD around 0.14 ns, exhibiting a significant improvement of 22% compared to the float solution. As for BDS-2 satellites, STD values exhibit variation among different products, ranging from the GBM's 0.14 ns to COM's 0.28 ns. This finding is also similar to the orbit comparison results, possibly due to the different SRP models employed by these institutions.

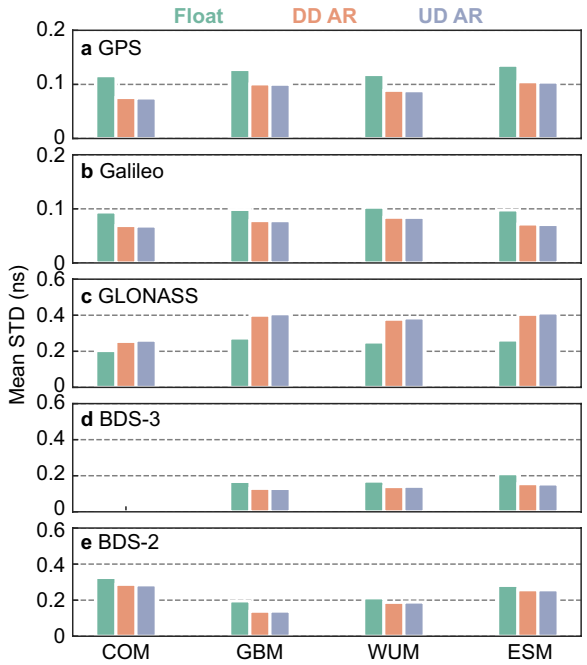

Fig. 14 Mean STD values of the clock difference in comparison with the final clock products from COM, GBM, WUM, and ESA (from left to right)

Furthermore, for GLONASS satellites the clock difference results are contrary to other systems. The STD values of GBM, WUM, and ESM exhibit substantial increment to about 0.40 ns when applying ambiguity resolution, representing a notable increase of 57% compared to the float solution. Nevertheless, the clock difference relative to COM shows a smaller STD value of 0.26 ns. This phenomenon likely stems from disparate ambiguity resolution strategies. Over all systems and different reference products, UD AR delivers the clock results with an accuracy comparable with DD AR, with discrepancies less than 3%.

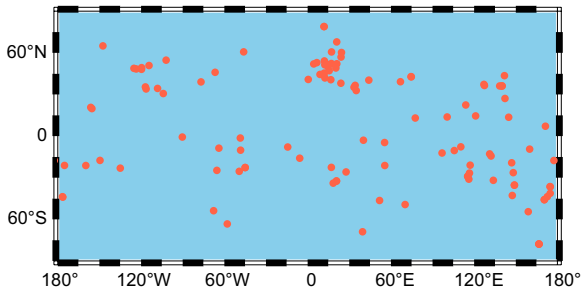

Fig. 15 Distribution of MGEX stations used for multi-GNSS kinematic PPP

PPP validation

To further assess the obtained quad-system precise orbit and IRC products, we utilize 120 globally distributed MGEX stations to execute GPS + BDS + Galileo + GLONASS kinematic PPP AR, as depicted in Fig. 15. Three PPP schemes are adopted: S1: the float PPP solution using the orbit and clock from the DD AR solution; S2: the same as S1 but using extra UPD products to facilitate PPP AR; S3: PPP AR using the orbit and IRC from UD AR solution. Both S2 and S3 use WL UPD products to fix WL ambiguities.

We utilized the LAMBDA method to search for the optimal integer ambiguity solution (Teunissen, 1995). Simultaneously, to resolve as many high-quality ambiguities as feasible we implemented the partially fixed integer solution by selecting high elevation or high precision ambiguities (Teunissen, 1999; Li & Zhang, 2015). Moreover, we used the ratio test for the acceptance of the integer solution with an empirical threshold of 2 (Han, 1997; Li et al., 2018). Furthermore, the reference coordinates were from the IGS weekly solutions.

Figure 16 illustrates the positioning errors for stations HARB, MKEA, and POVE in east, north, and up components. Notably, the ambiguity-fixed solutions (S2 and S3) manifest a faster convergence speed compared to the float solution, achieving centimeter-level accuracy within ten minutes. The improvement is particularly pronounced in the east components, from over ten minutes to several minutes. Between S2 and S3, the IRC-based AR solutions exhibit the convergence time and positioning errors similar to the UPD-based results.

Figure 17 illustrates the distributions of convergence time for all 120 stations. In this study, we defined the

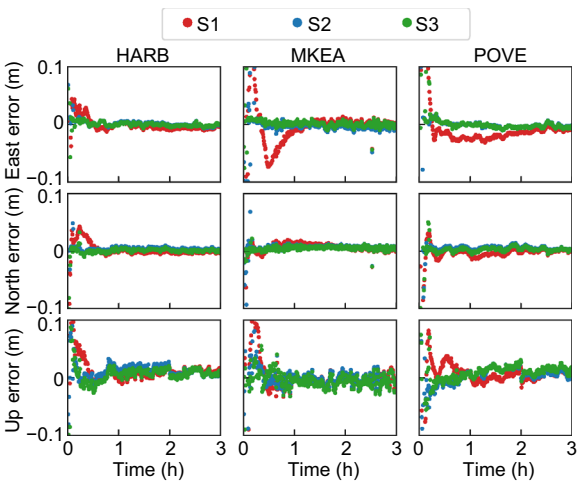

Fig. 16 Positioning errors for HARB, MKEA, and POVE stations in east, north, and up components in DOY241, 2020

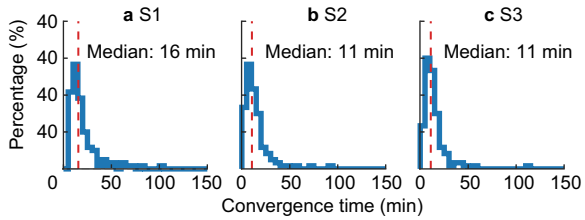

Fig. 17 Distributions of the convergence time for all 120 stations in DOY241, 2020

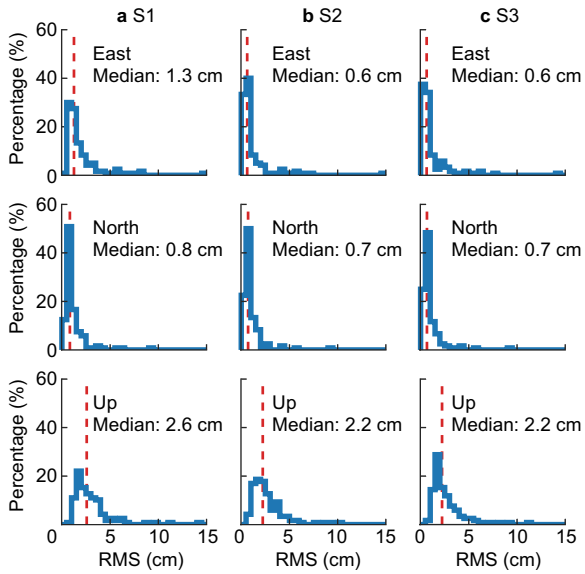

Fig. 18 Distributions of the positioning errors in east, north, and up components for all 120 stations in DOY241, 2020

convergence time as the duration required for the horizontal positioning accuracy to surpass the threshold of 5 cm and maintain for ten successive epochs. The distributions of ambiguity-fixed solutions (S2 and S3) manifest a pronounced skewness towards zero, with a median value of 11 min, contrasting 16 min with the float solution's (S1). Moreover, both S2 and S3 show an improvement of 31% in convergence time compared with the float solution.

Furthermore, we exam statistically the positioning errors, as illustrated in Fig. 18. The RMS values of six-hour positioning error is computed, with the first 30 min of the initialization time excluded. Notably, S3 achieves the median of positioning errors of 0.6, 0.7, and 2.2 cm in east, north, and up components, a comparable accuracy with that of S2. Compared with S1, the positioning accuracy is improved by 54%, 13%, and 15% in the east, north, and up components, respectively.

Conclusions

This contribution expounds upon the mathematical method, processing strategy, and validation results of the UD-ambiguity-fixed quad-system orbit and clock products from the iGMAS Wuhan IAC. Our approach converts raw phase observations to carrier ranges at a station by resolving integer UD ambiguities. Subsequently, the UD-ambiguity-fixed orbits and clocks are estimated based on these carrier range observations.

To validate the proposed method, the observations of one year at 150 MGEX stations in 2020 is employed. The quad-system WL UPDs manifests STDs of smaller than 0.02 cycles over the entire 2020, while the NL UPDs demonstrate daily STDs smaller than 0.05 cycles. Moreover, the success rate of ambiguity resolution with the UD method exhibits up to 9% higher than the traditional DD method, attributable to its avoidance of forming station baselines. Following this, the carrier range is generated at each station to facilitate the UD-ambiguity-fixed network solution. With the employment of carrier ranges, the computational efficiency of the parameter estimation for POD are significantly improved, particularly in the context of massive GNSS networks. When handling the GPS observations at 450 stations or a composite of GPS, Galileo, and BDS observations at 150 stations, the computational time required for equation formulation and matrix operations can be reduced by 30% and 70%, respectively.

Hence, the UD-ambiguity-fixed orbit products are assessed in terms of orbit consistency and orbit difference relative to precise products, and by SLR measurements. The 3D orbit fits RMS values are 1.9, 5.2, 2.8, 2.1, and 2.7 cm for GPS, BDS-2, BDS-3, Galileo, and GLONASS satellites, respectively, reflecting the improvements of 40%, 24%, 54%, 34%, and 42% compared to the float solution. The orbit fits are comparable with the traditional DD AR solution with the discrepancy smaller than 2%. The orbit differences with respect to the final products from COM, GBM, WUM, and ESM also exhibit the improvements of 30–50% compared to the float solution. Concerning SLR validation, the STD value of SLR residuals for BDS-3 satellites is reduced by 21%. Overall, the STD values of UD AR solutions range from 2.5 to 3.5 cm for MEO satellites, comparable to DD AR solution.

Furthermore, we evaluate the accuracy of IRC using the clock difference with respect to the precise products. The STDs of the clock differences for GPS and Galileo satellites span from 0.07 to 0.10 ns, while for BDS-3 satellites 0.14 ns. The IRC products enable single-receiver AR for global users, obviating the need for UPD products. We validate the performance of IRC-based kinematic PPP AR using 120 globally dispersed MGEX stations. Compared with the float solution, both the IRC-based PPP and UPD-based PPP achieve the convergence time of less

than 11 min, improved by 31%. The median positioning errors of IRC-based PPP are 0.6, 0.7, and 2.2 cm in east, north, and up components, with improvements of 54%, 13%, and 15% compared with the float solution.

Acknowledgements
The numerical calculations in this paper have been done on the supercomputing system in the Supercomputing Center of Wuhan University.

Author contributions
JW, XXL, and YY provided the initial idea and designed the experiments for this study; JW, XXL, YY, and KZ analyzed the data and wrote the manuscript; XL, JL, and YX helped with the writing. All authors reviewed the manuscript.

Funding
This study is financially supported by the National Natural Science Foundation of China (No. 42204017, No. 41974027, No. 42304019), the special fund of Hubei Luojia Laboratory (220100006), the Sino-German mobility program (Grant No. M-0054), China Postdoctoral Science Foundation (2023M732687), and the Fundamental Research Funds for the Central Universities (2042022kf1001).

Availability of data and materials
All data in this article are publicly accessible. The GNSS data and products can be obtained at https://cddis.nasa.gov/archive.

Declarations

Competing interests
Xingxing Li is the editorial board member of Satellite Navigation but was not involved in the review and decision processes to publish this article. The authors declare that they have no competing interests.

Author details
[1]School of Geodesy and Geomatics, Wuhan University, 129 Luoyu Road, Wuhan 430079, China. [2]Hubei Luojia Laboratory, 129 Luoyu Road, Wuhan 430079, China. [3]German Research Centre for Geosciences GFZ, Telegrafenberg, 14473 Potsdam, Germany. [4]Technische Universitat Berlin (TUB), Straße Des 17. Juni, 10623 Berlin, Germany.

Received: 18 August 2023 Accepted: 26 December 2023
Published online: 08 April 2024

References

Arnold, D., Meindl, M., Beutler, G., Dach, R., Schär, S., Lutz, S., Prange, L., Sósnica, K., Mervart, L., & Jäggi, A. (2015). CODE's new solar radiation pressure model for GNSS orbit determination. *Journal of Geodesy, 89*, 775–791.

Blewitt, G., Bertiger, W., & Weiss, J. P. (2010). Ambizap3 and GPS carrier-range: a new data type with IGS applications. In Proceedings of IGS Workshop and Vertical Rates, Newcastle, June, UK (Vol. 28).

Blewitt, G. (1989). Carrier phase ambiguity resolution for the Global Positioning System applied to geodetic baselines up to 2000 km. *Journal of Geophysical Research: Solid Earth, 94*(B8), 10187–10203.

Böhm, J., Niell, A., Tregoning, P., & Schuh, H. (2006). Global Mapping Function (GMF): A new empirical mapping function based on numerical weather model data. *Geophysical Research Letters*. https://doi.org/10.1029/2005GL025546

Bury, G., Sośnica, K., Zajdel, R., & Strugarek, D. (2022). GLONASS precise orbit determination with identification of malfunctioning spacecraft. *GPS Solutions, 26*(2), 36.

Chen, K., Xu, T., Chen, G., Li, J., Yu, S. (2015). The orbit and clock combination of iGMAS analysis centers and the analysis of their precision. *In China Satellite Navigation Conference (CSNC) 2015 Proceedings: II*. Springer, pp 421–438.

Chen, H., Jiang, W., Ge, M., Wickert, J., & Schuh, H. (2014). An enhanced strategy for GNSS data processing of massive networks. *Journal of Geodesy, 88*, 857–867.

Collins, P. (2008, January). Isolating and estimating undifferenced GPS integer ambiguities. *In Proceedings of the 2008 national technical meeting of the institute of navigation* (pp. 720–732).

Dach, R., Sušnik, A., Grahsl, A., Villiger, A., Schaer, S., Arnold, D., Prange, L., & Jäggi, A. (2019). Improving GLONASS orbit quality by re-estimating satellite antenna offsets. *Advances in Space Research, 63*(12), 3835–3847.

Dai, X., Gong, X., Li, C., Qing, Y., Gu, S., & Lou, Y. (2022). Real-time precise orbit and clock estimation of multi-GNSS satellites with undifferenced ambiguity resolution. *Journal of Geodesy, 96*(10), 73.

Deng, Z., Wang, J., & Ge, M. (2022, May). The GBM rapid product and the improvement from undifferenced ambiguity resolution. In *EGU General Assembly Conference Abstracts* (pp. EGU22–794).

Dong, D. N., & Bock, Y. (1989). Global positioning system network analysis with phase ambiguity resolution applied to crustal deformation studies in California. *Journal of Geophysical Research: Solid Earth, 94*(B4), 3949–3966.

Folkner, W. M., Williams, J. G., & Boggs, D. H. (2009). The planetary and lunar ephemeris DE 421. *IPN Progress Report, 42*(178), 1.

Ge, M., Chen, J., Douša, J., Gendt, G., & Wickert, J. (2012). A computationally efficient approach for estimating high-rate satellite clock corrections in realtime. *GPS Solutions, 16*, 9–17.

Ge, M., Gendt, G., Dick, G., & Zhang, F. P. (2005). Improving carrier-phase ambiguity resolution in global GPS network solutions. *Journal of Geodesy, 79*, 103–110.

Ge, M., Gendt, G., Dick, G., Zhang, F. P., & Rothacher, M. (2006). A new data processing strategy for huge GNSS global networks. *Journal of Geodesy, 80*, 199–203.

Ge, M., Gendt, G., Rothacher, M. A., Shi, C., & Liu, J. (2008). Resolution of GPS carrier-phase ambiguities in precise point positioning (PPP) with daily observations. *Journal of Geodesy, 82*, 389–399.

Geng, J., Chen, X., Pan, Y., & Zhao, Q. (2019). A modified phase clock/bias model to improve PPP ambiguity resolution at Wuhan University. *Journal of Geodesy, 93*, 2053–2067.

Geng, J., & Mao, S. (2021). Massive GNSS network analysis without baselines: Undifferenced ambiguity resolution. *Journal of Geophysical Research Solid Earth, 126*(10), e2020JB021558.

Guo, J., Xu, X., Zhao, Q., & Liu, J. (2016). Precise orbit determination for quad-constellation satellites at Wuhan University: Strategy, result validation, and comparison. *Journal of Geodesy, 90*, 143–159.

Hadas, T., Kazmierski, K., & Sośnica, K. (2019). Performance of Galileo-only dual-frequency absolute positioning using the fully serviceable Galileo constellation. *GPS Solutions, 23*(4), 108.

Han, S. (1997). Quality-control issues relating to instantaneous ambiguity resolution for real-time GPS kinematic positioning. *Journal of Geodesy, 71*, 351–361.

Hatch, R. (1983). The synergism of GPS code and carrier measurements. In *International geodetic symposium on satellite doppler positioning* (Vol. 2, pp. 1213–1231).

Katsigianni, G., Loyer, S., Perosanz, F., Mercier, F., Zajdel, R., & Sośnica, K. (2019). Improving Galileo orbit determination using zero-difference ambiguity fixing in a Multi-GNSS processing. *Advances in Space Research, 63*(9), 2952–2963.

Laurichesse, D. (2011, September). The CNES Real-time PPP with undifferenced integer ambiguity resolution demonstrator. In *Proceedings of the 24th International Technical Meeting of The Satellite Division of the Institute of Navigation (ION GNSS 2011)* (pp. 654–662).

Laurichesse, D., Mercier, F., Berthias, J. P., Broca, P., & Cerri, L. (2009). Integer ambiguity resolution on undifferenced GPS phase measurements and its application to PPP and satellite precise orbit determination. *Navigation, 56*(2), 135–149.

Li, P., & Zhang, X. (2015). Precise point positioning with partial ambiguity fixing. *Sensors, 15*(6), 13627–13643.

Li, X., Ge, M., Dai, X., Ren, X., Fritsche, M., Wickert, J., & Schuh, H. (2015). Accuracy and reliability of multi-GNSS real-time precise positioning: GPS, GLONASS, BeiDou, and Galileo. *Journal of Geodesy, 89*(6), 607–635.

Li, X., Ge, M., Zhang, H., & Wickert, J. (2013). A method for improving uncalibrated phase delay estimation and ambiguity-fixing in real-time precise point positioning. *Journal of Geodesy, 87*, 405–416.

Li, X., Han, X., Li, X., Liu, G., Feng, G., Wang, B., & Zheng, H. (2021). GREAT-UPD: An open-source software for uncalibrated phase delay estimation based on multi-GNSS and multi-frequency observations. *GPS Solutions, 25*, 1–9.

Li, X., Huang, J., Li, X., Shen, Z., Han, J., Li, L., & Wang, B. (2022a). Review of PPP–RTK: Achievements, challenges, and opportunities. *Satellite Navigation, 3*(1), 28.
Li, X., Li, X., Yuan, Y., Zhang, K., Zhang, X., & Wickert, J. (2018). Multi-GNSS phase delay estimation and PPP ambiguity resolution: GPS, BDS, GLONASS, Galileo. *Journal of Geodesy, 92*, 579–608.
Li, X., Wang, B., Li, X., Huang, J., Lyu, H., & Han, X. (2022b). Principle and performance of multi-frequency and multi-GNSS PPP-RTK. *Satellite Navigation, 3*(1), 7.
Li, X., Wang, Q., Wu, J., Yuan, Y., Xiong, Y., Gong, X., & Wu, Z. (2022c). Multi-GNSS products and services at iGMAS Wuhan Innovation Application Center: Strategy and evaluation. *Satellite Navigation, 3*(1), 20.
Li, X., Wu, J., Zhang, K., Li, X., Xiong, Y., & Zhang, Q. (2019a). Real-time kinematic precise orbit determination for LEO satellites using zero-differenced ambiguity resolution. *Remote Sensing, 11*(23), 2815.
Li, X., Yuan, Y., Huang, J., Zhu, Y., Wu, J., Xiong, Y., Li, X., & Zhang, K. (2019b). Galileo and QZSS precise orbit and clock determination using new satellite metadata. *Journal of Geodesy, 93*, 1123–1136.
Li, X., Zheng, H., Li, X., Yuan, Y., Wu, J., & Han, X. (2023). Open-source software for multi-GNSS inter-frequency clock bias estimation. *GPS Solutions, 27*(2), 84.
Liu, Y., Song, W., Lou, Y., Ye, S., & Zhang, R. (2017). GLONASS phase bias estimation and its PPP ambiguity resolution using homogeneous receivers. *GPS Solutions, 21*, 427–437.
Loyer, S., Perosanz, F., Mercier, F., Capdeville, H., & Marty, J. C. (2012). Zero-difference GPS ambiguity resolution at CNES–CLS IGS Analysis Center. *Journal of Geodesy, 86*, 991–1003.
Luzum, B., & Petit, G. (2012). The IERS Conventions (2010): Reference systems and new models. *Proceedings of the International Astronomical Union, 10*(H16), 227–228.
Lyard, F., Lefevre, F., Letellier, T., & Francis, O. (2006). Modelling the global ocean tides: Modern insights from FES2004. *Ocean Dynamics, 56*, 394–415.
Melbourne, W. G. (1985). The case for ranging in GPS-based geodetic systems. In *Proceedings of the first international symposium on precise positioning with the Global Positioning System* (pp. 373–386), April. US Department of Commerce Rockville, Maryland.
Montenbruck, O., Hackel, S., Wermuth, M., & Zangerl, F. (2021). Sentinel-6A precise orbit determination using a combined GPS/Galileo receiver. *Journal of Geodesy, 95*(9), 109.
Montenbruck, O., Steigenberger, P., & Hugentobler, U. (2015). Enhanced solar radiation pressure modeling for Galileo satellites. *Journal of Geodesy, 89*, 283–297.
Montenbruck, O., Steigenberger, P., Prange, L., Deng, Z., Zhao, Q., Perosanz, F., & Schaer, S. (2017). The Multi-GNSS Experiment (MGEX) of the International GNSS Service (IGS)–achievements, prospects and challenges. *Advances in Space Research, 59*(7), 1671–1697.
Pavlis, N. K., Holmes, S. A., Kenyon, S. C., & Factor, J. K. (2012). The development and evaluation of the Earth Gravitational Model 2008 (EGM20408). *Journal of geophysical research: solid earth*. https://doi.org/10.1029/2011JB008916
Pearlman, M. R., Noll, C. E., Pavlis, E. C., Lemoine, F. G., Combrink, L., Degnan, J. J., et al. (2019). The ILRS: approaching 20 years and planning for the future. *Journal of Geodesy, 93*, 2161–2180.
Prange, L., Orliac, E., Dach, R., Arnold, D., Beutler, G., Schaer, S., & Jäggi, A. (2017). CODE's five-system orbit and clock solution—the challenges of multi-GNSS data analysis. *Journal of Geodesy, 91*, 345–360.
Ruan, R., & Wei, Z. (2019). Between-satellite single-difference integer ambiguity resolution in GPS/GNSS network solutions. *Journal of Geodesy, 93*(9), 1367–1379.
Saastamoinen, J. (1972). Contributions to the theory of atmospheric refraction. *Bulletin Géodésique (1946–1975), 105*(1), 279–298.
Schaer, S., Villiger, A., Arnold, D., Dach, R., Prange, L., & Jäggi, A. (2021). The CODE ambiguity-fixed clock and phase bias analysis products: Generation, properties, and performance. *Journal of Geodesy, 95*, 1–25.
Springer, T. A., Beutler, G., & Rothacher, M. (1999). A new solar radiation pressure model for GPS satellites. *GPS Solutions, 2*, 50–62.
Steigenberger, P., Thoelert, S., & Montenbruck, O. (2018). GNSS satellite transmit power and its impact on orbit determination. *Journal of Geodesy, 92*(6), 609–624.
Temiissen, J. G. (1995). The least-squares ambiguity decorrelation adjustment: A method for fast GPS integer ambiguity estimation. *Journal of Geodesy, 70*, 65–82.
Teunissen, P. J. G., Joosten, P., & Tiberius, C. C. J. M. (1999). Geometry-free ambiguity success rates in case of partial fixing. In *Proceedings of the 1999 national technical meeting of the institute of navigation*, January (pp. 201–207).
Teunissen, P. J. G., & Khodabandeh, A. (2015). Review and principles of PPP-RTK methods. *Journal of Geodesy, 89*(3), 217–240.
Uhlemann, M., Gendt, G., Ramatschi, M., & Deng, Z. (2016). GFZ global multi-GNSS network and data processing results. *In IAG 150 Years: Proceedings of the IAG Scientific Assembly in Postdam, Germany, 2013* (pp. 673–679). Springer International Publishing.
Wanninger, L., & Beer, S. (2015). BeiDou satellite-induced code pseudorange variations: Diagnosis and therapy. *GPS Solutions, 19*, 639–648.
Wübbena, G. (1985, April). Software developments for geodetic positioning with GPS using TI-4100 code and carrier measurements. In *Proceedings of the first international symposium on precise positioning with the global positioning system* (Vol. 19, pp. 403–412). US Department of Commerce Rockville, Maryland.
Yamada, H., Takasu, T., Kubo, N., & Yasuda, A. (2010). Evaluation and calibration of receiver inter-channel biases for RTK-GPS/GLONASS. In *Proceedings of the 23rd international technical meeting of the Satellite Division of the Institute of Navigation (Ion GNSS 2010)*, September (pp. 1580–1587).
Yang, Y., Liu, L., Li, J., Yang, Y., Zhang, T., Mao, Y., Sun, B., & Ren, X. (2021). Featured services and performance of BDS-3. *Science Bulletin, 66*(20), 2135–2143.
Zhang, K., Li, X., Wu, J., Yuan, Y., Li, X., Zhang, X., & Zhang, W. (2021). Precise orbit determination for LEO satellites with ambiguity resolution: improvement and comparison. *Journal of Geophysical Research: Solid Earth, 126*(9), e2021JB022491.
Zhao, Q., Guo, J., Wang, C., Lyu, Y., Xu, X., Yang, C., & Li, J. (2022). Precise orbit determination for BDS satellites. *Satellite Navigation, 3*(1), 2.
Zhao, W., Chen, H., Gao, Y., Jiang, W., & Liu, X. (2020). Evaluation of inter-system bias between BDS-2 and BDS-3 satellites and its impact on precise point positioning. *Remote Sensing, 12*(14), 2185.

Publisher's Note